Understanding the Edge Physics of Divertor Experiments by Comparison of 2-D Edge Code Calculations and Experimental Measurements

A. Loarte

JET Joint Undertaking, Abingdon, Oxon., OX14 3EA, UK

ABSTRACT.

A review on the assessment of the models contained in 2-D plasma edge codes by comparing their results with experimental measurements of the SOL and divertor plasma is presented. Improvements in the models and experimental measurements in recent years have allowed a quantitative assessment of the predictions of the codes in a wide variety of regimes. In particular the accuracy of these codes to evaluate the effects of divertor geometry, reproduce experimental observations of divertor detachment, ELMs, Marfes and radiative H-mode discharges is described in detail. Areas where further experimental measurements and model improvements need to be carried out are highlighted.

1. INTRODUCTION.

The problems of erosion and heat load on plasma-facing materials have been identified as one of the main areas to be addressed in the design of present day divertor experiments and next step devices such as ITER [1]. Presently, the favoured solutions to these problems are based on the extrapolation of the radiative divertor regimes observed in experiments [2,3,4,5,6,7,8], where divertor volumetric losses (hydrogenic and impurity radiation, charge exchange, etc.) reduce the power and the ion flux to the divertor target achieving the so-called detached divertor regime.

Sophisticated 2-D plasma fluid codes coupled to Monte Carlo or fluid codes for neutral species [9,10,11,12,13] have been developed to perform realistic calculations of the divertor and scrape-off layer (SOL) plasma parameters. These codes have been significantly improved in recent years by including adequate models for many of the atomic physics processes that occur in the divertor region and scrape-off layer [14] and a proper description of the divertor target geometry, allowing the study of geometrical effects of the divertor design on its performance [15,16,17].

The basic equations contained in all these codes are based on a simple prescription for the anomalous plasma transport across the field (specifying the transport coefficients) and classical parallel plasma transport for electrons, hydrogenic and impurity ions along the field. The equations for parallel transport follow Braginskii's formulation, usually including flux limits for the momentum and energy fluxes, in order to account for kinetic effects, which are important when the scale length of the variation of plasma parameters along the field is comparable to the relevant mean free paths. Transport in the SOL and divertor is influenced by classical drifts, in particular the asymmetries between the divertors, and these have been included in most codes to several degrees of sophistication. The subject of drifts in the SOL is treated in a separate paper [18] and will not be discussed here. However, it must be stressed that some of the difficulties encountered in the modelling reviewed in this paper are likely to be related to the effect of drifts, which are seen to strongly influence the SOL and divertor in existing experiments [19,20,21]. For a review of the models and the numerics used in the 2-D codes for the plasma edge the reader is referred to [22] and references therein.

In this paper we summarise the recent results from the comparison of the predictions of these 2-D codes with various experiments. The reader is referred to the paper by Neuhauser et al. [23] as a representative study of the research status of this field at the end of the last decade.

2. GENERAL APPROACH AND PROBLEMS IN MODELLING OF EXPERIMENTS AND TESTS OF BASIC ASSUMPTIONS CONTAINED IN 2-D EDGE CODES.

2.1. Experimental Uncertainties and Modelling of Experiments.

The aim of the modelling process is to reproduce with the 2-D codes those plasma and neutral parameters measured in the SOL and divertor thereby drawing conclusions on other physical processes which affect divertor performance and are difficult to directly measure in the experiments (such as plasma flows). The results of 2-D code calculations are also used to help understand the experimental measurements themselves, which are often integrated along lines of sight where plasma parameters vary substantially and, hence, cannot be interpreted in a simple way.

The first step in modelling a discharge consists of generating a mesh in which the calculations will be performed. This mesh is produced from the calculated magnetic equilibrium for the discharge and should also contain detailed information on the material structures inside the vacuum chamber, which affect the neutral transport in the region between the plasma and the vacuum vessel wall. Divertor by-pass leaks that allow neutrals to back-stream from the divertor into the main chamber, must be properly incorporated into the calculations. These leakage paths cannot be neglected as divertors become more closed and the direct neutral leakage from the divertor to the bulk plasma decreases.

The basic inputs to the 2-D codes which are varied to fit the experiment are :

- Input power into the computational domain (and proportion shared by electrons and ions). It is assumed to come out from the bulk plasma by anomalous diffusion.

- Plasma density at the magnetic separatrix (or other closed flux reference surface).
- Anomalous perpendicular diffusion coefficients for the transport of particles ($D_\perp$) and electron and ion energy ($\chi_\perp^e$, $\chi_\perp^i$). These are adjusted to match the measured shape of the upstream SOL density and temperature profiles.

Simultaneous with this iterative matching process, the measured radiation due to impurities in the SOL must also be incorporated in the calculations, so that meaningful comparisons of the upstream and divertor plasma parameters can be performed. The modelling of this radiation is usually done at two levels of sophistication : a) Assuming a constant impurity fraction in the SOL and calculating the associated radiation with a non-coronal approximation [24,25] or b) Full multispecies description of all of the ions in the plasma together with the radiation rates for all impurity ionisation stages from collisional-radiative model calculations [25,26,27].

We will now discuss the various uncertainties involved in the process described above, taking as an example the UEDGE modelling result for a DIII-D ELMy H-mode [28] (Fig. 1 and Fig. 2). The main problem in modelling the upstream profiles is related to the uncertainty in the absolute position of the measured profiles with respect to the magnetic separatrix. In most tokamaks this is typically 1 cm at the outer midplane and comparable to the measured e-folding length for the temperature and density profiles. This uncertainty influences not only the values of the temperature and density which are used to match the code to the experiment, but also the values of the diffusion coefficients used to achieve this. The energy transport is particularly sensitive, as the measured temperature gradients near the separatrix change quite abruptly in its vicinity [29], and the calculation aim also to reproduce the experimental power balance. The different criteria (discussed later) followed by various modelling\experimental groups for the determination of the separatrix position may be strongly linked with the variation of the effective transport coefficients reported in the literature.

A further uncertainty in the modelling process is due to the difficulties involved in measuring the ion temperature in the SOL and divertor. Without this data, the power outflux from the main plasma into the ion and electron channels and the ion heat diffusion coefficient can be varied to fit the experiment, but no direct comparison with measured ion parameters is possible. Charge-Exchange spectroscopy data of the SOL ion temperature is available for some DIII-D discharges and, from UEDGE modelling of these, it has been concluded [30] that the assumption of equal SOL power sharing between ions and electrons is valid for ELMy H-mode discharges. This, together with the fact that the ion temperature shows a flatter profile in the SOL (Fig. 1), results in the ion heat diffusion coefficient being larger than the electron heat diffusion coefficient ($\chi_\perp^i \approx 1.5 - 2\,\chi_\perp^e$) [30]. In the absence of ion temperature data, the power is assumed to flow out of the main plasma equally shared by the electrons and the ions and values of $\chi_\perp^{\,i} \approx \chi_\perp^{\,e}$ are typically used. With these prescriptions it is possible to obtain a reasonable match to experiment in Ohmic, L-mode and ELMy H-mode discharges. The only regime that deviates strongly from this is the Hot-ion H-mode in JET, where the measured electron power reaching the divertor is much smaller than that derived from power balance [31]. In [32] it was shown that this discrepancy could be resolved by assuming that most of the power flows out the plasma via the ion channel. This has been confirmed by simulations of discharges in the JET Mark I divertor where improved IR power deposition measurements are available [33].

The determination of the particle diffusion coefficient $D_\perp$, is even more uncertain than that of the $\chi_\perp$'s, due to the existence of large ionisation sources in the SOL. The value of $D_\perp$ used in the 2-D codes is not only influenced by the separatrix position but also by assumptions about the particle recycling coefficient at the surfaces exposed to ion and neutral flux. The values of the recycling coefficients are not uniform within the modelling community and are also influenced by the type of model used to describe the hydrogenic neutral transport. In UEDGE modelling of DIII-D with fluid neutrals, the recycling coefficient is set to a value (0.985 - 1.0, at the divertor and 0.95 elsewhere) consistent with the ionisation source in the main plasma, derived from the density increase at the L-H transition [30]. For 2-D codes with neutral Monte Carlo transport, albedos are used to characterise the pumping provided in the experiment by the vacuum vessel pumps and the vessel walls. These albedoed particles are restored in the balance by a "gas puff", in the same way as in the experiment, and the ionisation source in the plasma is determined consistently [10,11].

Hence, in order to confirm that the choice of separatrix position and transport coefficients is correct, additional information is needed. This is usually provided by comparing the calculated and measured parameters at the divertor target, where the uncertainties in magnetic geometry are smaller than at the midplane. The parameters to compare depend on the experimental information available : in the example shown in Figs. 2 and 3, the power deposition and H_α emission from the divertor are compared with the calculations. The reasonable agreement proves that both the separatrix position choice and energy transport/losses along the field line are properly described.

Different criteria are used to adjust the separatrix position in various experiments. In ASDEX [23] and JET modelling [15], the prescription is based on the approximate conservation of electron pressure, measured by Langmuir probes, along the field. This criteria has the advantage that it does not depend on the energy transport/losses along the field. However, it cannot be applied to detached phases of discharges, where the electron pressure is no longer conserved along the field, unless a reference exists for attached phases of the same discharge. The separatrix position in Alcator C-mod from MHD equilibria calculations is determined with a higher precision than in other machines (maybe related to machine size) and no further adjustment is necessary [34]. In this case, a factor of two ratio in electron pressure (measured by Langmuir probes) between the main SOL and the divertor is found experimentally. The difference in the electron pressure ratio in various experiments is probably related to the different ratio of the electron to ion temperature in these experiments. The measurement of the electron pressure with Langmuir probes assumes implicitly that the electron and ion temperatures are comparable. For regimes with higher ion than electron temperature, the electron pressure from Langmuir probes is an overestimate of the real electron pressure. Hence, the absence of ion temperature measurements in the SOL also introduces some degree of uncertainty in the electron pressure balance method.

With all the caveats that the previous discussion implies, it is routinely found with all the codes that small values of the diffusion coefficients must be used to reproduce the steep profiles measured in the experiment. Typical values used to model various regimes are in the range [28,30,32,35,36,37] : $D_\perp = 0.1 - 0.3\ m^2/s$, $\chi_\perp^{e,i} = 0.5 - 2.0\ m^2/s$, for Ohmic discharges, $D_\perp = 0.1 - 0.5\ m^2/s$, $\chi_\perp^{e,i} = 1.0 - 5.0\ m^2/s$, for L-mode discharges, and $D_\perp = 0.05 - 0.2\ m^2/s$, $\chi_\perp^{e,i} = 0.1 - 0.5\ m^2/s$ for H-mode discharges. These ranges summarise results for 2-D codes applied to various machines and some of the variations that they contain are probably associated with differences between codes more than real differences in the experiments. Nevertheless, it gives a good indication of the values of the effective transport coefficients characteristic of SOL transport.

2.2. Tests of Basic Assumptions Contained in the 2-D Edge Codes.

The models implemented in 2-D codes contain a series of physical assumptions which are difficult to directly test experimentally. Some of them are unlikely to be ever tested experimentally, such as the boundary conditions imposed by the sheath to the ions flowing to the target. However, new experimental measurements are presently allowing the detailed test of the accuracy of some of other basic assumptions contained in the 2-D codes :

2.2.1. Electron Parallel Heat Transport.

Until recently, the electron parallel heat transport could only be assessed by comparing the measurements of the electron temperature at two locations (i.e. midplane and divertor), with the associated problems of the separatrix position uncertainty already discussed. New divertor diagnostics, such as the Divertor Thomson scattering in DIII-D [38] and the Thermal Helium beam in JET [39], have allowed a more detailed comparison of the electron temperature gradients within the divertor region, where the magnetic geometry is known accurately. These results have shown that the measured gradients are compatible with those computed from classical transport. Fig. 3 (from calculations in [40]) shows such a comparison of the measured and computed divertor temperature with UEDGE for a DIII-D discharge.

2.2.2. Particle and Energy Anomalous Transport.

In most of the 2-D codes, the perpendicular particle and energy transport is assumed to be diffusive in the SOL and characterised by constant diffusion coefficients, whose values are adjusted to match the experiment. This prescription for the energy diffusion coefficients seems to describe well the measured temperature profiles in the main SOL along with the power deposition and temperature profiles at the divertor for all confinement regimes. The same prescription for the particle diffusion coefficient can describe well the measured density profiles in most machines, including discharges of low to medium density in JET. However, for discharges that achieve the divertor high recycling regime in JET, very peaked density profiles have been measured at the divertor [45]. These profiles cannot be reproduced by EDGE2D/U-NIMBUS with a simple constant diffusion coefficient across the SOL. A possible way to reproduce these profiles is by including an inward particle pinch in the SOL, similar to that identified in the main plasma, or by a substantial reduction of the transport in the private flux region, such as the one associated with a Bohm-type scaling that depends on the local electron temperature. A comparison of such EDGE2D/U-NIMBUS calculations using a constant diffusion coefficient and an inward SOL particle pinch with the experimentally determined ion flux profiles is shown in Fig. 4 [46]. The nature of these high recycling peaks is not well understood and intermediate stages of their evolution in the experiment show clear double peaked structures [45] that cannot be explained with the present models; they may be related to classical drifts, which are not included in the modelling presented here.

2.2.3. Impurity Production and Transport.

The area of impurity production and transport is even more complex than that of deuterium transport. The reader is referred to another review paper in these proceedings for progress in this area [41]. It is worth noting the general agreement between all modelling groups, in the need for chemical sputtering to explain the production of carbon at least in areas of low incident particle flux, such as the inner wall [42] and private flux region of the divertor [43]. The existence of these low energy carbon atoms has been confirmed in [36], and it is necessary to explain the steep decay of the carbon emission away from the divertor along the field line. However, the relation between carbon source and radiation emitted by the several impurity ionisation stages is far from being tested accurately. Work is in progress to experimentally test the radiation efficiencies derived from collisional-radiative models and the UV emission of the various ionisation stages in the divertor plasma (such a study for JET is presented in [44]). These uncertainties lead to difficulties in evaluating absolute impurity levels in the plasma, as in many cases their absolute level in the 2-D codes is determined by matching the level of radiation measured in the experiment. It is also a cause for discrepancies between the results of modelling groups that use atomic data of different origin.

3. MODELLING OF DIVERTOR DETACHMENT.

The detached divertor regime [2,3,4,5,6,7,8] is characterised by a low peak ion flux to the divertor target and high H_α emission from the divertor region. These observations are usually accompanied by high neutral pressures measured in the divertor region, together with large radiative losses in the divertor and X-point region. The possibility of achieving these large radiative losses and low peak ion flux to the divertor target makes this regime very attractive to operate a divertor tokamak reactor such as ITER [47]. Since the original paper by Watkins and Rebut [48], where the first proposal was made to ameliorate the problem of the power deposition on the divertor plate, by extinguishing the divertor plasma with charge-exchange neutral energy losses, a substantial research activity has taken place in the experimental, theoretical and modelling areas. It was soon shown that hydrogen charge-exchange and recycling losses alone are insufficient to extinguish the plasma [49 , 50, 51] and impurity radiation must play an important role. However, charge-exchange and elastic collisions between the ions flowing to the plate and the recycling atoms and molecules have been identified as important processes in the momentum loss (pressure drop along the field) observed to take place in divertor detachment [52], [53]. For a review of the present status of understanding of divertor detachment the reader is referred to [54].

3.1. Experimental Observations.

Firstly, we describe the basic observations of plasma detachment using an example of a JET discharge (Fig. 5) and then we will discuss the modelling of the processes believed to account for the experimental observations. The divertor plasma evolves through three distinct states as the main plasma density increases (more experimental details can be found in [3, 5, 34, 55, 56]): At low main plasma density the divertor is in the low recycling regime, which is characterised by low ion fluxes and high electron temperatures at the divertor (similar to those at the separatrix in the main SOL) and, hence, the divertor density is low. As the main plasma density increases, the divertor ion flux increases strongly and the electron temperature decreases, achieving the so-called high recycling regime with high divertor plasma density. For both of these regimes, the pressure balance between the upstream SOL and divertor plasma is maintained [34,55]. Once the separatrix divertor temperature has reached very low values (3 - 5 eV), the divertor pressure ceases to increase (roll-over phase) and, if the density increases further, starts to decrease, first close to the separatrix and extending towards the outer part of the SOL. This is the so-called detached divertor regime where the total plasma pressure is no longer constant along the field but decreases strongly at the divertor plate. During this process, the neutral pressure in the divertor private flux region and the H_α emission from the divertor continue to increase with the main plasma density.

3.2. Modelling of Divertor Detachment : Momentum Removal.

The proposed mechanism for the momentum loss (pressure drop) in the divertor is the friction between the ions flowing to the divertor target and the recycling neutrals coming from it, through charge-exchange and elastic scattering collisions [52]. The momentum losses associated with these interactions have been implemented in the fluid codes by coupling to Monte Carlo neutral codes [10,11] or fluid neutral codes [37,57]. The evaluation of the plasma -neutral momentum transfer is different in these two approaches : in fluid neutral models momentum is removed from the plasma by neutrals through a diffusive process; Monte Carlo calculations include this effect implicitly, but also account for direct losses of momentum by neutrals reaching the wall after the first neutral-ion interaction. For an ion temperature of 5 eV and divertor density of 10^{20} m^{-3}, the charge-exchange mean free path is approximately 2 cm and, hence, both momentum removal mechanisms can be significant [54].

The calculated momentum losses with either approach are similar to those deduced from the experimental SOL/divertor pressure drop [46, 37, 58], at least for intermediate stages in the evolution towards total detachment. An example of such calculations is shown in Fig. 6,for a JET L-mode discharge modelled with EDGE2D/U-NIMBUS. In this case, the outer divertor is still attached and the pressure balance method is used to determine the position of the measured upstream profiles with respect to the magnetic separatrix. However, the inner divertor has reached the roll over phase and the measured electron pressure there is about a factor of 5 lower than at the outer divertor. This pressure drop is reproduced by the calculations which include radiation losses in the divertor and SOL following [24], adjusted to the level measured in the experiment. The inner divertor electron temperature from Langmuir probes is approximately 3-6 eV, while in code calculations is 1-4 eV. These somewhat large values of the inner divertor temperature are typical for JET discharges, and it is thought that these measurements suffer from resistive effects which lead to an overestimation of the electron temperature [59]. The precise value of the electron temperature at detachment is crucial in determining which physical processes are involved and will be discussed further below. The calculated average neutral flux in the JET subdivertor module is 6.5 x 10^{21} atoms/m^2s (equivalent to a neutral pressure of 0.46 x 10^{-3} mb) which compares well with the measured flux at the cryopump of 10^{22} atoms/m^2s (equivalent to a neutral pressure of 0.72 x 10^{-3} mb). In these calculations a neutral leakage from the subdivertor module to the main chamber of 8.6 10^{21} atoms/s (4 % of the total ion and neutral flux on the divertor, and similar to the radial ion flux out of the computational grid onto the walls), must be allowed for, in order to reproduce the measured H_α emission in the main chamber (10^{14} ph/sr cm^2 s).

3.3. Modelling of Divertor Detachment : Recombination.

Momentum losses by ion-neutral interactions can explain the pressure drop along the field observed in divertor detachment but cannot explain by themselves the reduction in total ion flux to the divertor seen in advanced phases of detachment, in which the upstream pressure remains at similar levels than during high recycling, as seen in Alcator C-mod [34] and JET [56]. This is illustrated in Fig. 7, for EDGE2D/U-NIMBUS and UEDGE simulations of a density scan in typical JET L-mode conditions [60]. Momentum losses by ion-neutral interactions prevent the total ion divertor flux from increasing with main plasma density but on their own do not reduce significantly total ion divertor flux.

From detailed analysis of similar calculations, Borrass [61,63] concluded that plasma recombination must take place at some stage of divertor detachment in order to explain the drop in total ion flux to the divertor. Experimental evidence indicates that two different kind of processes takes place as detachment progresses. Fig. 8 shows the evolution of the peak and integrated ion flux to the divertor during an ohmic density ramp to detachment in JET together with the results from EDGE2D/U-NIMBUS simulations. The behaviour of the inner and outer divertors is clearly different : inner divertor detachment leads to a drop in the peak and integral ion flux; however, the outer divertor integrated ion flux shows just a small decrease after roll-over, although its peak can decrease significantly as the ion flux profiles broaden. This decrease of the integrated ion flux is reproduced by the codes only if recombination is included, although the inner divertor electron temperature (1 eV) is much lower than that measured (3-5 eV), with the caveat of possible resistive effects in these measurements [59].

Further experimental evidence that points towards recombination taking place at same stage of divertor detachment comes from hydrogen visible spectroscopy. The D_α emission for the inner and outer divertors in JET shows a very different behaviour : while for the outer divertor the ratio of the total ion flux to D_α emission changes from 25 at low/high recycling to 5 at detachment, for the inner divertor it changes from 25 at low/high recycling to 0.2 at detachment. This very low ratio of the inner divertor total ion flux to D_α can be only reproduced by the calculations if the contribution of recombination to the D_α emission is included. Similarly, the ratio for D_γ to D_α emission from the inner divertor increases as detachment proceeds. This is consistent with the occurrence of processes that populate the levels of hydrogen excited states in a different way than electron collisions, as recombination does. Fig.9 [74] shows the calculated D_γ/D_α ratio including and neglecting recombination compared to the measurements for a similar ohmic density ramp to detachment in JET. Although the calculated values including recombination overestimate the increase of this ratio, the trend agrees with the experiment.

The description for JET given above is qualitatively consistent with the other experiments. However, the degree of detachment reached depends on the experiment and probably the divertor geometry. For instance, the description of detachment at the JET outer divertor is in good agreement with DIII-D observations [40], but not with Alcator C-mod experiments, in which the integrated ion flux decreases significantly [34], and electron temperatures of 1 eV in the detachment region are measured. These observations are consistent with recombination taking place also at the outer divertor, in agreement with UEDGE modelling [37] and measurements of continuum emission and hydrogen line ratios [64]. All the simulations that describe the decrease of the total ion flux at detachment use as recombination mechanism radiative or/and three body recombination, but this assumption has to be properly verified. The mechanism that can account for the "measured" recombination depends critically on the divertor electron temperature. Reported values of the electron temperature at the outer divertor are in the range of 1-3 eV at detachment [34, 55, 40, 56], while at the inner divertor the only reported values come from JET and are in the range of 3-5 eV [56], with the caveat of the influence of resistive effects. Although the difference between 1 and 3 eV seems small, it is unfortunately crucial in determining the recombination mechanism. For example, the radiative and three body recombination rate coefficient for hydrogen changes by an more than an order of magnitude in this range, for typical plasma conditions [14], while it does not change significantly if it is driven by molecular processes [62]. Careful analysis of the hydrogen emission spectra should be used to identify the precise process that takes place in the experiment [64], although selective re-absorption in optically thick plasmas may further complicate the analysis [14]. While the recombination mechanism remains uncertain, it is difficult to assess the relative part played by momentum losses and recombination in the phenomena observed at plasma detachment.

3.4. Modelling of Divertor Detachment : Impurity Behaviour.

A typical observation that accompanies detachment is the movement of the radiation and the impurity density maximum from the divertor target towards the X-point [66]. This is reproduced by all of the 2-D codes [40, 46, 58], an example of the migration of the impurity maximum from calculations similar to those in [46] is shown in Fig. 10. The main forces on impurities involved in this balance are the thermal force that drives the impurities away from the target and the friction with the deuterium ions that flow towards the recombination front, which is situated near the X-point for these simulations. The final position of the radiation in the 2-D code calculations depends on assumptions about the perpendicular transport (and possibly drifts) and the mechanisms involved in impurity production (carbon in most cases). Here, there are differences between various modelling groups : EDGE2D/U-NIMBUS simulations for JET require a 1.5% chemical sputtering yield at all vessel surfaces to account for the measured radiation during detachment; similar values of the chemical sputtering yield lead to radiative collapse in ASDEX-Upgrade simulations [58] and this coefficient must be reduced by at least an order of magnitude to simulate the experiment. This highlights differences related to the various sources of atomic data, for which a thorough experimental assessment of their validity is urgently needed.

The strong radiative energy sink in the X-point vicinity causes the electron temperature to drop to low values (under 5 eV) in the region between the X-point and the divertor. This prediction has been recently confirmed experimentally by divertor Thomson scattering measurements in DIII-D which show a large region of very low temperature (under 7 eV) that at detachment extends to a distance of 5 - 10 cm from the divertor target [40].

4. MODELLING OF DIVERTOR GEOMETRY EFFECTS AND COMPARISON WITH THE EXPERIMENT.

One of the major enhancements in the 2-D codes implemented in recent years is the ability to model divertor plates which intersect the magnetic field line at very glancing poloidal angles [10, 17, 67]. Experiments with this type of divertor geometry have been performed at Alcator C-Mod and JET with the Mark I divertor and more are planned in the near future (JET Mark IIA divertor, ASDEX-Upgrade Lyra divertor , DIII-D advanced divertor). The basic idea of this divertor design is based on the effect that the geometry of the divertor plates has upon the recycling neutrals (Fig. 11). While for standard horizontal divertors the recycling neutrals are directed towards the outer part of the SOL, for vertical plate divertors the recycling neutrals are directed towards the separatrix. This recycling pattern enhances the ionisation near the separatrix and with it the volumetric losses (charge-exchange, ionisation, radiation) from this region, which lowers the plasma temperature at the separatrix. This lower temperature leads to a lower power flux at the separatrix, where power fluxes are greatest, and is predicted to allow access to detachment at lower main plasma densities for the vertical plate configuration, as compared to the horizontal divertor.

A study of this effect with EDGE2D/U-NIMBUS for typical conditions in the JET Mark I divertor was carried out in [16] and the results summarised in Fig. 12. In this figure, the pressure drop between the midplane and the divertor (f_p) is plotted as a function of the upstream SOL density, for the separatrix and the line at 1cm from it, at the midplane. These calculations show clearly that the vertical plate divertor accesses the regime of separatrix detachment ($f_p >> 1$) at much lower values of the upstream density than the horizontal plate. However, the trend is inverted for the outer part of the SOL (1cm-line) reflecting the effect of the divertor geometry on recycling. An extensive series of experiments was carried out in JET to compare both divertor configurations. Although some of the predicted geometry effects were found, no large differences in the approach to detachment for both configurations were seen in the experiment [68]. The reasons for this discrepancy between predictions and the experiment are twofold :

- The Mark I divertor structure is made of rows of tiles pairs with toroidal gaps in between. These can account for 10 - 20% of the divertor surface area and were not included in the calculations in [16]. Such gaps are effective in redistributing the neutral flux under the divertor structure, and hence masking, the detailed effect of the geometry, as proven in the JET experiments on pumping [69]. Substantial neutral by-pass leaks from the sub-divertor module to the main chamber have been identified [70], which reduce considerably the divertor closure to neutrals (4% is needed to account for the main chamber H_α in the simulations of section 3).

- The existence of a region of reduced particle transport in the private flux region and/or a SOL particle pinch produces peaked density profiles also for horizontal plate divertors as shown in [46], and correspondingly decreases the influence of the details of neutral recycling on the accessibility to the high recycling and detachment regime.

In contrast to JET experience, experiments in Alcator C-mod are in agreement with the expected trends [71]. For Ohmic discharges, it has been found that detachment can be achieved at a lower main plasma density (a factor of 2) if the divertor strike point is located on the vertical plate of the divertor than if it is located on the horizontal plate. Furthermore, it is not possible to obtain detachment in the external part of the horizontal plate (beyond the so-called ''divertor nose") for either divertor configuration. This finding is also in good agreement with the geometrical effects included in the models [37]. The reasons for the differences between JET and Alcator C-mod are not clear and are probably related to the larger divertor closure of Alcator C-mod which leads to higher neutral pressures in the divertor.

Other features expected for the recycling pattern associated with a vertical plate divertor are in better agreement with the results of 2-D codes. One such effect is the existence of a region of over - pressure near the separatrix, in which the divertor total plasma pressure (static plus dynamic) exceeds the plasma pressure at the midplane. This phenomena has been identified experimentally in Alcator C-mod [72] and in code calculations with B2-EIRENE [73] (Fig. 13) and EDGE2D/U-NIMBUS [74]. The reason for this over-pressure in the calculations is the viscous transfer of momentum from the outer part of the SOL where, because of geometry effects, the ions are hotter and flow faster to the divertor target (due to the sheath boundary condition), to the separatrix, where the temperature (and flow speed to the divertor) is low.

Another phenomena associated with the effect of a vertical divertor on recycling is the existence of a region of flow reversal close to the separatrix. Flow reversal is predicted to occur when the ionisation of neutrals in a flux tube exceeds the particle losses through the sheath and has been observed in divertor tokamaks [75]. Because of geometrical effects, the vertical divertor is particularly prone to produce flow reversal in this region. Flow reversal has been measured in Alcator C-mod discharges with a scanning Mach probe that enters the scrape-off layer above the X-point [76]. A comparison of the predicted pattern in Alcator C-mod for the ion flow Mach number at the probe position from EDGE2D/U-NIMBUS simulations and the measurement is shown in Fig. 14. The calculated and measured flow pattern across the SOL are in good qualitative agreement : reversed flow close to the separatrix and strong flow towards the divertor further out in the SOL. However, the calculated flow Mach number and the extent of the region of reversed flow do not agree quantitatively with the experiment. In the experiment, both the flow Mach number and the reversed flow region are found to depend on the direction of the toroidal field [76] and hence on drifts, which are not included in these calculations.

5. MODELLING OF TIME DEPENDENT PHENOMENA : ELMS & MARFES.

In order to study neutral transport in a rapidly changing background plasma, the Monte Carlo code EIRENE has been modified into a time dependent code [77]. This version of the code coupled to B2 has been extensively used to model time dependent phenomena in the SOL, such as Marfes[78] and ELMs [79,80,81].

The time dependent evolution of Marfes in the code is followed by an implemented feedback loop that adjust the hydrogen gas puff to keep a pre-set level of radiation, in a similar way as it can be done in the experiment [78]. With this method, it is possible to reproduce the non-linear evolution of the Marfe state, going through regimes where the radiation exceeds 100% of the input power, and study the bi-stable behaviour of this phenomena, where two solutions exists with a Marfe and Marfe free state for the same value of the controlling gas puff.

The structure of the Marfe depends quite sensitively on assumptions about the mechanisms of perpendicular transport and becomes more spatially concentrated if Bohm-like transport is assumed instead of constant diffusion coefficients. The particle and momentum flux equilibrium in the Marfe are established by the strong recirculation of deuterium ions. The force balance for the lower ionisation stages is dominated by the thermal force, which drives the low charged ions towards the Marfe against the friction with the higher ionisation stages. For high ionisation stages, the thermal force changes sign and hence they are driven away from the Marfe. The main result of this complicated flow pattern is that the Marfe is established by a 2-D deuterium recirculation flow, driven purely by parallel and perpendicular transport [78] and not by the ionisation and recombination of deuterium, in striking contrast to the detached divertor plasmas discussed in section 3.

The technique used to simulate ELMs with B2-EIRENE consists of increasing the perpendicular transport coefficients, during a short time interval, in a region of few centimetres inside of the separatrix and in the SOL, with the same frequency as the ELMs in the experiment [79]. The values of the transport coefficients used in these Type I ELM simulations are of $D_\perp$ = 0.5 m^2/s, $\chi_\perp$ = 0.1 m^2/s between ELMs and are increases to 5 m^2/s at the ELM. The period of increased transport was varied in this study [79,81] and it was found that a duration of 1ms for this period could describe satisfactorily the observed power flux, ion flux and H_α emission from the divertor. Increasing transport coefficients only inside of the separatrix produces very peaked power deposition profiles, which are much narrower than the ones measured in the experiment [80,81] (Fig. 15). This is consistent with the ELM causing an ergodization of the flux surfaces in the vicinity of the separatrix in the main plasma and the SOL. As a result of the transport increase, the density profile broadens considerably, its e-folding length increasing from 1.5 cm between ELMs to 7 cm during the ELMs. This increased density SOL width during the ELM and the duration of the enhanced transport phase is also substantiated by the evolution of the coupling resistance of the ICRF antenna during Type I ELMs in ASDEX-Upgrade [82].

However, there are some ELM observations that cannot be explained by a large increase of the transport at the ELM, such as the multiply peaked power deposition profiles that have been measured at JET [83]. These are believed to be linked to the distortion of the divertor magnetic field structure during the ELM and should not be interpreted as a profile broadening, consequence of an enhanced cross-field transport at the ELM.

Similar studies for type III ELMs in radiative H-modes [58, 80] show that the length of the enhanced transport phase must be reduced to 100 μs to reproduce the experimental features. The effect of these ELMs in the impurity production and radiation has also been studied in detail for discharges in highly radiative regimes [58,80] discussed in the following section

6. MODELLING OF ITER RELEVANT REGIMES : RADIATIVE H-MODES.

One of the main objectives of 2-D code development and of the comparison with experiments is to assess the accuracy of the models that they contain, so that these codes can be used to predict divertor performance in next step machines. For this reason, it is very important to compare the results of these 2-D codes with experimental regimes that have good confinement and large radiative losses such as those envisaged for ITER [47]. These regimes are achieved in existing experiments by low Z impurity and deuterium puffing into ELMy H-mode discharges [7,8]. These discharges are modelled by increasing the impurity density (and the impurity radiation) with a feed-back loop, until the measured level is achieved, in a similar way as in the experiment. Extensive simulations of these experimental regimes has been performed with the time dependent B2-EIRENE [58,80] for ASDEX-Upgrade discharges and with EDGE2D/U-NIMBUS for some JET discharges.

The overall characteristics of these regimes in ASDEX-Upgrade are well reproduced by B2-EIRENE, in particular the pressure drop along the field line, characteristic of detachment, and also good agreement between the calculated and measured neutral flux under the divertor and measured radiation is found. The contribution of carbon and neon radiation to the total measured is somewhat more uncertain, because it depends on the accuracy of the radiation efficiencies used and the yield for carbon production, mainly by chemical sputtering due to the low temperature at the plate (less than 3 eV). A more complete study than that of [58] for these discharges was described in [80], where the domain of the computations was extended to the plasma centre and a scan of the influence of the value of the chemical sputtering yield was performed. The transport coefficients used for these calculations for the main plasma were obtained from BALDUR simulations and adjusted to $D_\perp = 0.2\ m^2/s$, $\chi_\perp = 0.5\ m^2/s$ few cm inside of the separatrix and in the SOL, being increased to 5 m^2/s in the whole domain during the duration of the ELM (100 μs). With these prescriptions, it is possible to reproduce qualitatively the experimental behaviour of the CII emission from the divertor, where an oscillatory behaviour of the emission cloud that jumps between the X-point and the divertor is observed [58]. In the study performed in [80], it was found that a better match of the total radiation is achieved by using a chemical sputtering yield of 0.5% instead of the 2% used in [58]. It is important to note that although the radiation is reproduced, the calculated carbon emission from the plate by visible spectroscopy (CII, 657.8 nm) is considerably higher (a factor of 4-10 at the ELM) than that measured for high neon radiation cases, even with a 0.1% chemical sputtering yield. This leads to the radiation in the calculations being dominated by Carbon (2.3 MW) even for cases with high Neon radiation (1.6 MW) and low chemical sputtering yield (0.1%), in contrast to the experiment.

The most important effects found in these calculations are related to the movement of the radiation cloud and to the enhancement of the transient radiative losses in the SOL and divertor at the ELM [58,80]. As shown in Fig. 10 and in agreement with the experiment, as the plasma detaches the radiation tends to move towards the X-point and, at high radiative fractions, forms a Marfe in the main plasma which leads to the collapse of the 2-D code solutions. However, when the ELM is triggered in the calculations, the radiation moves closer to the divertor target (from the X-point vicinity) which allows higher radiative losses in the code to be obtained than without the effect of the ELMs, not developing a main plasma Marfe. The same dynamic behaviour of the radiation is seen in the experiment [58,80] and, hence, this predicted stabilising effect of the ELMs on the radiation can explain the experimental stability of discharges with high radiative fractions.

The increase of particle transport during the ELM, together with the temperature rise at the midplane (an increase of 10 eV), enhances the radiative losses in the SOL and divertor. In this way, the increased power flux into the SOL associated with ELM is radiated away by the impurities (carbon and neon in these calculations) before it reaches the divertor plate, in good agreement with the experimental evidence. The two main effects that contribute to the enhanced radiation losses are the increase of SOL impurity density and density SOL width, associated with the enhanced ELM transport, and the ionisation of low charged impurity ions because of the temperature increase that the ELM causes. Fig. 16 shows the calculated time evolution of such losses during an ELM, where the outer divertor radiation can increase from 1.0 MW between ELMs to 2.7 MW at the ELM peak and in the SOL from 1.5 MW between ELMs to 3.8 MW at the ELM peak. The average losses by deuterium, carbon and neon are also shown in this figure and are consistent with the experimental observation that neon tends to radiate more in the SOL and the edge of the main plasma, while carbon radiates closer to the divertor, as expected from their characteristic cooling rates. Simulations for JET ELMy H-mode discharges with nitrogen puffing have been carried out with EDGE2D/U-NIMBUS. Good agreement with the measurements of radiated power, ion flux to the divertor, divertor neutral pressure and divertor H_α emission are obtained by using large values of the diffusion coefficients ($D_\perp = 0.4$ m^2/s, $\chi_\perp = 2.5$ m^2/s), which is probably related to the fact that ELMs are not included in these simulations. However, the measured nitrogen concentration in the main plasma, as derived from the Z_{eff}, is a factor of 3-4 larger than that calculated by the 2-D code. Whether this is due to profile effects in the Z_{eff} or to discrepancies between the real radiation efficiency of nitrogen and that estimated from the atomic database is unclear.

A point of great interest in these type of regimes is to determine how well the divertor retains the impurities and how this experimental retention compares with 2-D code predictions. The compression of impurities in the divertor can be characterised by the ratio of the impurity density in the divertor to that in the main plasma and, hence, has the advantage of not being so dependent on the absolute impurity density as the total radiation. Calculations of the compression ratio for neon and helium have been performed for ASDEX-Upgrade discharges and the results are in good agreement with the experiment (Fig. 17) being lower for helium than for neon. A strong increase of this compression is observed as the neutral flux in the divertor increases (i.e. main plasma density increases) and, together with it, the divertor retention increases and the transparency of the SOL to impurities decreases. The helium compression is worse in code and experiment as expected from its higher ionisation potential, which leads to its de-enrichment in the divertor as compared to hydrogen. The JET experiments show a larger value of the compression (measured and calculated) for nitrogen in similar regimes. For a neutral gas flux density in the divertor of 1.2×10^{22} D_2 molec/m^2s, the compression factor derived from the experiment using the technique described in [84] is 15(±5) while from code calculations is 20. The reasonable agreement between experimental and calculated impurity compression with B2-EIRENE and EDGE2D/U-NIMBUS is very encouraging and seems to indicate that the impurity transport in these regimes is well described by the models contained in these 2-D codes.

7. AREAS WHERE FURTHER WORK IS NEEDED.

Although there has been considerable progress in the quantitative assessment of the models contained in the 2-D SOL codes, there is still much work to be done to reach the level of confidence in their accuracy that will facilitate their use as a tool for detailed divertor design.

Some of the remaining areas to explore need additional experimental information, while some other need model improvements and testing. The following is a selected list of items of immediate interest to assess or improve the model/experiment comparison :

- Ion temperature measurements in the SOL and Divertor. Lack of these measurements prevents the check of some basic modelling assumptions, such as the relative power sharing between electrons and ions and the assessment of the ion temperature gradients along the field. Unfortunately, the ion temperature is a very important parameter with respect to impurity production and transport, through the thermal force on impurities. Without these measurements, the accuracy of the impurity production and transport models contained in the 2-D codes cannot be properly assessed.

- Impurity and Hydrogen Radiative losses. It is of crucial importance to carry out a detailed experimental assessment of the measured divertor radiative losses by hydrogen and impurities with the calculated ones [44]. Without such studies, it is difficult to determine if discrepancies found by comparison between the measured and calculated radiation and the measured and calculated impurity source are due to inaccuracies in the atomic models or problems in the impurity transport models.

- Anomalous transport and drifts. The description of the anomalous transport in the SOL is fairly primitive in most of the codes. This simplicity is in sharp contrast with the level of sophistication in the parallel transport models for deuterium ions and impurities. Recent experimental evidence highlights the need for more sophisticated models to describe the profiles measured in the SOL and divertor [46]. A successful method, used in JET, to identify discrepancies between code and experiment is based in the comparison of code and experimental scans of one plasma parameter. For instance, a low density discharge is modelled in detail with the code and, once a satisfactory description of the perpendicular transport for that discharge is identified, a density scan is performed with the code and compared to the same experimental scan. In this way, without further adjustment of knobs in the code, striking differences between calculations and experiment are routinely found [68], which are used to identify the areas where code improvements are needed. Classical drifts are also estimated to influence SOL plasma transport and have been included in the 2-D codes, with various degrees of sophistication [85, 86, 67]. Numerous studies have been performed to determine their influence in the experiment [19, 20, 21], but an accurate comparison of 2-D code predictions and experimental results has not yet been carried out [18].

- Divertor Detachment mechanisms. In the last year, it has become apparent that momentum loss by neutral-ion friction does not provide an explanation for all the experimental observations of divertor detachment, such as the reduction of total ion flux to the divertor. This observation can be explained if the ions recombine before they reach the divertor plate. Two mechanisms are proposed for divertor recombination : radiative/dielectronic recombination and molecule catalysed recombination [62]. The identification of the recombination process is crucial in order to assess the relative role of momentum loss with neutrals and recombination in the detachment process.

- Processes in high neutral density divertors. As divertors evolve towards a greater closure to neutrals, the divertor neutral densities increase. Therefore, new physical processes must be included in the 2-D codes which are relevant at neutral densities of $> 10^{20}$ m^{-3}, such as neutral-neutral collisions and radiation transport in the optically thick divertors. The neutral-neutral mean free path at these densities is few centimetres (comparable to divertor dimensions) and, hence, neutral-neutral interactions can affect significantly the divertor behaviour [57]. At these densities, the mean free path for a L_α photon is shorter than 2 mm and the divertor will be optically thick to hydrogen radiation, which not only affects the radiation losses from hydrogen but also its ionisation balance [14]. Experimental observations in C-mod and JET have shown radiation trapping for L_β [87,88] (which has a mean free path one order of magnitude larger than L_α) and, hence, these processes have to be incorporated into 2-D codes to model the existing experiments.
- Coupling of core transport and 2-D edge codes. The description of the core plasma in the 2-D plasma edge codes is also rather primitive (it is simply taken as a boundary condition). It is well known that processes at the plasma edge significantly influence the transport in the main plasma and, hence, the need to link the description of the edge transport with the main plasma transport. Some attempts in this direction have already been carried out, either by linking 2-D edge codes to main plasma transport codes [89,90] or by extending the 2-D mesh of the edge code towards the plasma centre (using transport coefficients from main plasma transport codes) [80]. The link between the edge and bulk transport is a very promising activity but up to present no systematic comparison with the experiment has been performed.

8. CONCLUSIONS.

A substantial effort has been dedicated in recent years to the quantitative assessment of the models contained in the 2-D codes for the plasma edge. These codes can reproduce satisfactorily many of the measured plasma characteristics of divertor experiments such as parallel temperature gradients for attached plasmas, the pressure drop along the field line characteristic of plasma detachment, flow reversal for vertical divertor configurations, etc., which are discussed in this paper. However, many experimental observations remain unexplained by these models such as the asymmetry between divertors and its dependence of toroidal field direction, and the level of agreement in some predictions such as the relation between the measured/computed impurity source to measured/computed radiation is not accurate enough. Substantial work lies ahead to test the accuracy of these 2-D codes to the point at which they can be used as a tool for detailed divertor design. Until this point is reached, these 2-D codes may be used to evaluate relative merits of different divertor designs but the confidence in their predictions must not be overestimated.

9. ACKNOWLEDGEMENTS.

This review has been made possible with the help and contributions of many of those working in the area of divertor research. I am particularly grateful to the following persons for their contributions, encouragement and helpful discussions : M. Baelmans, K. Borrass, S. Bosch, S. Clement, S. Cohen, D. Coster, G. Corrigan, P. Harbour, L. Horton, N. Hosogane, I. Hutchinson, Y. Igithkanov, K. Itami, G. Janeschitz, C. Karney, S. Krasheninnikov, A. Kukushkin, B. La Bombard, J. Lingertat, B. Lipschultz, C. Maggi, G. Matthews, G. McCracken, R. Monk, J. Neuhauser, N. Ohyabu, F. Perkins, G. Porter, D. Post, D. Reiter, T. Rognlien, G. Saibene, R. Schneider, M. Shimada, R. Simonini, J. Snipes, R. Stambaugh, P. Stangeby, M. Sugihara, A. Taroni, J. Terry, G. Vlases and J. Winter.

10. REFERENCES.

[1] P.H Rebut, et al., Fusion Eng. and Design 22 (1993) 7.

[2] S. Clement, et al., 33th Conf. Am. Phys. Soc. Plasma Phys. Div., Tampa, USA, 1991, JET Report JET-IR(91)11.

[3] T. Petrie, et al., J. Nucl. Mater. 196-198 (1992) 848.

[4] G. Janeschitz, et al., Controlled Fusion and Plasma Physics (Proc. 19th Eur. Conf. Innsbruck, Austria, 1992), vol. 16C, part II, p.727.

[5] M. Laux, et al., Controlled Fusion and Plasma Physics (Proc. 20th Eur. Conf. Lisboa, Portugal, 1993), vol. 17C.

[6] I. Hutchinson, et al., Phys. Plasmas 1 (1994) 1511.

[7] O. Gruber, et al., Phys. Rev. Lett. 74 (1995) 4217

[8] JET Team (G.F. Matthews), Plasma Phys. Control. Fusion 37 (1995) A227.

[9] B. Braams, NET Report no. 68 . EUR-FU/XII-80/87/68, CEC (1987).

[10] R. Simonini, et al., Contrib. Plasma Phys. 34 (1994) 448

[11] D. Reiter, et al., Plasma Phys. Control. Fusion 33 (1991) 1579.

[12] T. D. Rognlien, et al., J. Nucl. Mater., 196-198 (1992) 347.

[13] N. Ueda, et al., Contrib. Plasma Phys. 34 (1994) 350

[14] D.E. Post, J. Nucl. Mater. 220-222 (1995) 143.

[15] JET Team (G. Vlases), Proc 14th IAEA Conf. Plasma Phys. and Contr. Nucl. Fusion Res., vol. 1 (1992) 287.
[16] A. Taroni, et al., J. Nucl. Mater. 220-222 (1995) 1086.
[17] R. Schneider, et al., J. Nucl. Mater. 220-222 (1995) 1076.
[18] A. Chankin, Proc. 12th PSI Conference, Saint Rapha'l, France, 1996.
[19] M. Laux, et al., Controlled Fusion and Plasma Physics (Proc. 22th Eur. Conf. Bournemouth, United Kingdom, 1995), vol. 19C, part III, p.97.
[20] A. Chankin, et al., Controlled Fusion and Plasma Physics (Proc. 22th Eur. Conf. Bournemouth, United Kingdom, 1995), vol. 19C, part III, p.289.
[21] I. H. Hutchinson, et al., Plasma Phys. Control. Fusion 37 (1995) 1389.
[22] D. Reiter, J. Nucl. Mater. 220-222 (1992) 80.
[23] J. Neuhauser, et al., Plasma Phys. Control. Fusion 31 (1989) 1551.
[24] J. Neuhauser et al., Nucl. Fusion 26 (1986) 1679.
[25] R. Hulse et al., Jour. Phys. B 3 (1980) 3895.
[26] K. Behringer, JET Report JET-R(87)08, Joint European Torus, 1987.
[27] H.P. Summers, JET Report JET-IR(94)06, Joint European Torus, 1994.
[28] M. E. Fenstermacher et al., Jour. Nucl. Mat. 220 -222 (1995) 330.
[29] G. D. Porter, et al., Contrib. Plasma Phys. 34 (1994) 454.
[30] G. D. Porter, Proc 15th IAEA Conference on Plasma Physics and Controlled Nuclear Fusion Research, Sevilla, Spain, 1994, Paper IAEA-CN-60/D-P-I-1.
[31] A. Loarte. PhD Thesis. Universidad Complutense de Madrid, Spain, 1992.
[32] A. Loarte et al., Jour. Nucl. Mat. 220 - 222 (1995) 606.
[33] K. G. McCormick et al., Proc. 12th PSI Conference, Saint Rapha'l, France, 1996.
[34] B. LaBombard, et al., Phys. Plasmas 6 (1995) 2242.
[35] S. Tsuji et al., Jour. Nucl. Mat. 220 - 222 (1995) 400.
[36] H-S. Bosch, et al, Jour. Nucl. Mat. 220 - 222 (1995) 558.
[37] F. Wising, et al., Proc 5th Plasma Edge Theory Workshop, Asilomar, USA, 1995. To be Published in Contrib. Plasma Phys., 1996.
[38] T.N. Carlstrom, et al., Rev. Sci. Instrum., 66 (1995) 493.
[39] S.J. Davies, et al, Proc. 12th PSI Conference, Saint Rapha'l, France, 1996.
[40] G.D. Porter, et al., 37th Conf. Am. Phys. Soc. Plasma Phys. Div., Louisville, USA, 1995. To be published in Phys. Plasmas, 1996.
[41] K. Shimizu, Proc. 12th PSI Conference, Saint Rapha'l, France, 1996.
[42] G.F. Matthews, et al., J. Nucl. Mater. 196-198 (1992) 374.
[43] K. Shimizu, et al., Proc 15th IAEA Conference on Plasma Physics and Controlled Nuclear Fusion Research, Sevilla, Spain, 1994, Paper IAEA-CN-60/D-P-I-2.
[44] C.F. Maggi, et al., Proc. 12th PSI Conference, Saint Rapha'l, France, 1996.
[45] R.D. Monk, et al., Proc. 12th PSI Conference, Saint Rapha'l, France, 1996.

[46] A. Taroni, et al., Controlled Fusion and Plasma Physics (Proc. 22th Eur. Conf. Bournemouth, United Kingdom, 1995), vol. 19C, part IV, p.297.

[47] G. Janeschitz, et al., J. Nucl. Mater. 220-222 (1995) 73.

[48] M. L. Watkins and P. H. Rebut, Controlled Fusion and Plasma Physics (Proc. 19th Eur. Conf. Innsbruck, Austria, 1992), vol. 16C, part II, p.731.

[49] R. Schneider, et al., Controlled Fusion and Plasma Physics (Proc. 20th Eur. Conf. Lisboa, Portugal, 1993), vol. 17C, part II, 775.

[50] S. Weber, et al., Controlled Fusion and Plasma Physics (Proc. 20th Eur. Conf. Lisboa, Portugal, 1993), vol. 17C, part II, p.767.

[51] A. Taroni, et al., Contrib. Plasma Phys. 34 (1994) 448.

[52] P.C. Stangeby, Nucl. Fusion (1993) 1695.

[53] K. Borrass, P. C. Stangeby, Controlled Fusion and Plasma Physics (Proc. 20th Eur. Conf. Lisboa, Portugal, 1993), vol. 17C, part II, 763.

[54] S.I. Krasheninnikov, Proc 5th Plasma Edge Theory Workshop, Asilomar, USA, 1995. To be Published in Contrib. Plasma Phys., 1996.

[55] B. Lipschultz, et al., J. Nucl. Mater. 220-222 (1995) 51.

[56] R.D. Monk, et al., Controlled Fusion and Plasma Physics (Proc. 22th Eur. Conf. Bournemouth, United Kingdom, 1995), vol. 19C, part III, p.293.

[57] D. A. Knoll, et al., Phys. Plasmas 3 (1996) 293.

[58] R. Schneider, et al., Controlled Fusion and Plasma Physics (Proc. 22th Eur. Conf. Bournemouth, United Kingdom, 1995), vol. 19C, part IV, p.285, and ITER Divertor Physics and Modelling and Database Expert Group, 1995, Naka, Japan.

[59] K. Günther, Controlled Fusion and Plasma Physics (Proc. 22th Eur. Conf. Bournemouth, United Kingdom, 1995), vol. 19C, part I, p.433.

[60] G.D. Porter, A. Loarte, Private Communication, 1995.

[61] K. Borrass, private communication, JET 1995.

[62] S.I. Krasheninnikov, et al., MIT Report PFC/JA-95-37, 1995.

[63] K. Borrass, et al., Proc. 12th PSI Conference, Saint Rapha'l, France, 1996.

[64] J. Terry, et al., To be published

[65] T. Fujimoto, ITER Divertor Physics and Modelling and Database Expert Group, 1996, San Diego, USA.

[66] G.F. Matthews, J. Nucl. Mater. 220-222 (1995) 104.

[67] T.D. Rognlien, et al., Proc 5th Plasma Edge Theory Workshop, Asilomar, USA, 1995. To be Published in Contrib. Plasma Phys., 1996.

[68] A. Loarte, et al., Controlled Fusion and Plasma Physics (Proc. 22th Eur. Conf. Bournemouth, United Kingdom, 1995), vol. 19C, part III, p.305.

[69] G. Saibene, et al., Controlled Fusion and Plasma Physics (Proc. 22th Eur. Conf. Bournemouth, United Kingdom, 1995), vol. 19C, part II, p.121.

[70] P.J. Harbour, JET, Private Communication, 1996.

[71] B. Lipschultz, et al., Controlled Fusion and Plasma Physics (Proc. 22th Eur. Conf. Bournemouth, United Kingdom, 1995), vol. 19C, part III, p.325.

[72] B. La Bombard, IPP-DoE Divertor Workshop, Garching, Germany, 1995.

[73] R. Schneider, ITER Divertor Physics and Modelling and Database Expert Group, 1996, San Diego, USA.

[74] A. Loarte, ITER Divertor Physics and Modelling and Database Expert Group, 1996, San Diego, USA.

[75] L. De Kock, et al., Proc 12th IAEA Conf. Plasma Phys. and Contr. Nucl. Fusion Res., vol. 1 (1988) 467.

[76] B. Lipschultz, ITER Divertor Physics and Modelling and Database Expert Group, 1996, San Diego, USA.

[77] D. Reiter, et al., J. Nucl. Mater. 220-222 (1995) 987.

[78] H. Kastelewicz, et al., Plasma Phys. Control. Fusion 37 (1995) 723.

[79] D.Coster, et al., Controlled Fusion and Plasma Physics (Proc. 21th Eur. Conf. Montpellier, France, 1994), vol. 18C, part II, p.846.

[80] D. Coster, et al., 37th Conf. Am. Phys. Soc. Plasma Phys. Div., Louisville, USA, 1995.

[81] D. Coster, et al., Proc 5th Plasma Edge Theory Workshop, Asilomar, USA, 1995. To be Published in Contrib. Plasma Phys., 1996.

[82] J. M. Noterdaeme, et al., Controlled Fusion and Plasma Physics (Proc. 21th Eur. Conf. Montpellier, France, 1994), vol. 18C, part II, p.842.

[83] J. Lingertat, et al., Proc. 12th PSI Conference, Saint Rapha'l, France, 1996.

[84] J. K. Ehrenberg, et al., Proc. 12th PSI Conference, Saint Rapha'l, France, 1996.

[85] M. Baelmans, et al., J. Nucl. Mater. 220-222 (1995) 982.

[86] G. Radford, et al., to be published.

[87] B. Lipschultz, ITER Divertor Physics and Modelling and Database Expert Group, 1995, Naka, Japan.

[88] T. Lovegrove, et al., Controlled Fusion and Plasma Physics (Proc. 22th Eur. Conf. Bournemouth, United Kingdom, 1995), vol. 19C, part III, p.301.

[89] M. Baelmans, et al., Controlled Fusion and Plasma Physics (Proc. 22th Eur. Conf. Bournemouth, United Kingdom, 1995), vol. 19C, part IV, p.321.

[90] A. Taroni, et al., Proc 5th Plasma Edge Theory Workshop, Asilomar, USA, 1995. To be Published in Contrib. Plasma Phys., 1996.

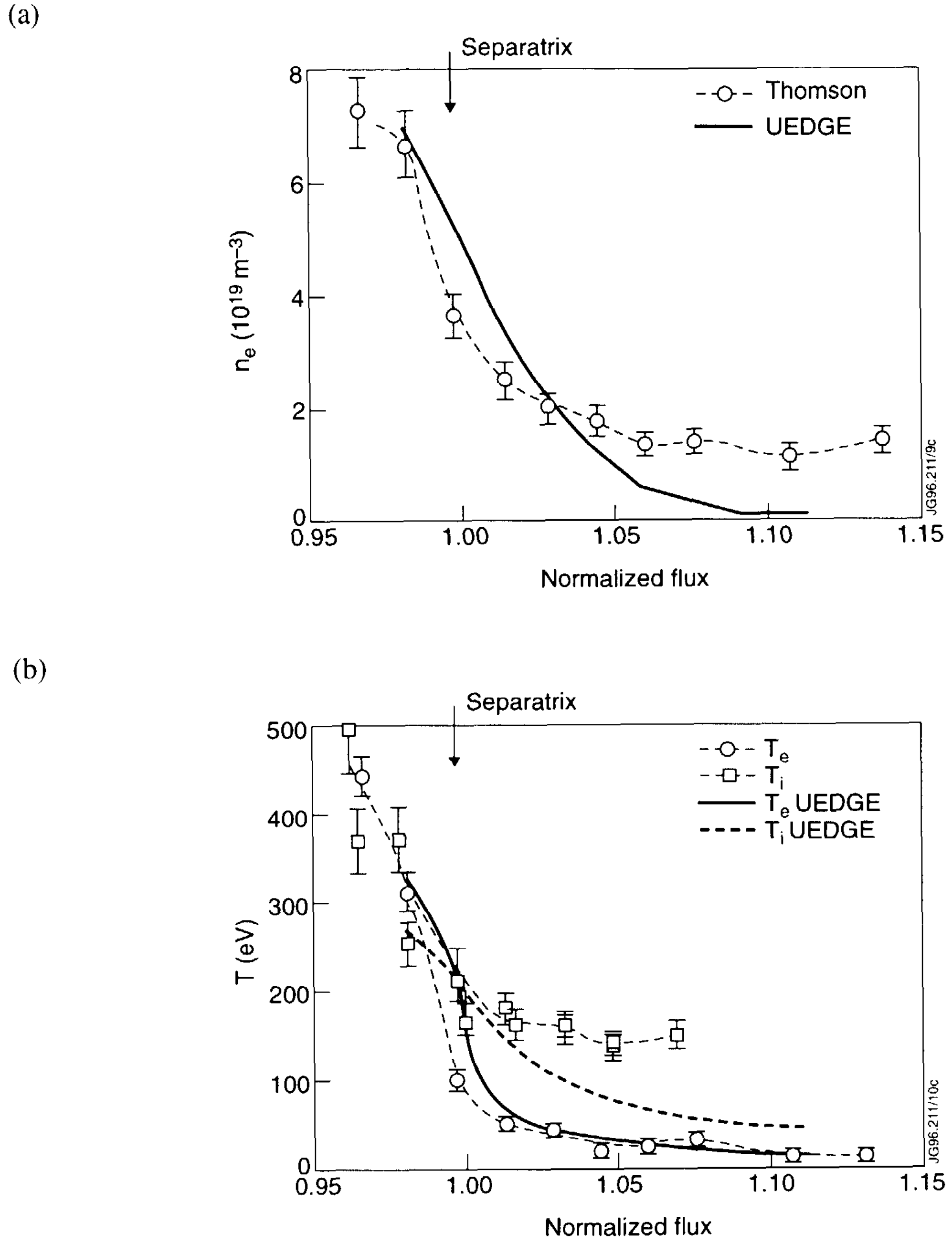

Fig.1.a. Upstream measured and UEDGE modelled density profiles for a DIII-D ELMy H-mode discharge versus normalised magnetic flux. b. Upstream measured and UEDGE modelled electron and ion temperature profiles for a DIII-D ELMy H-mode discharge versus normalised magnetic flux.

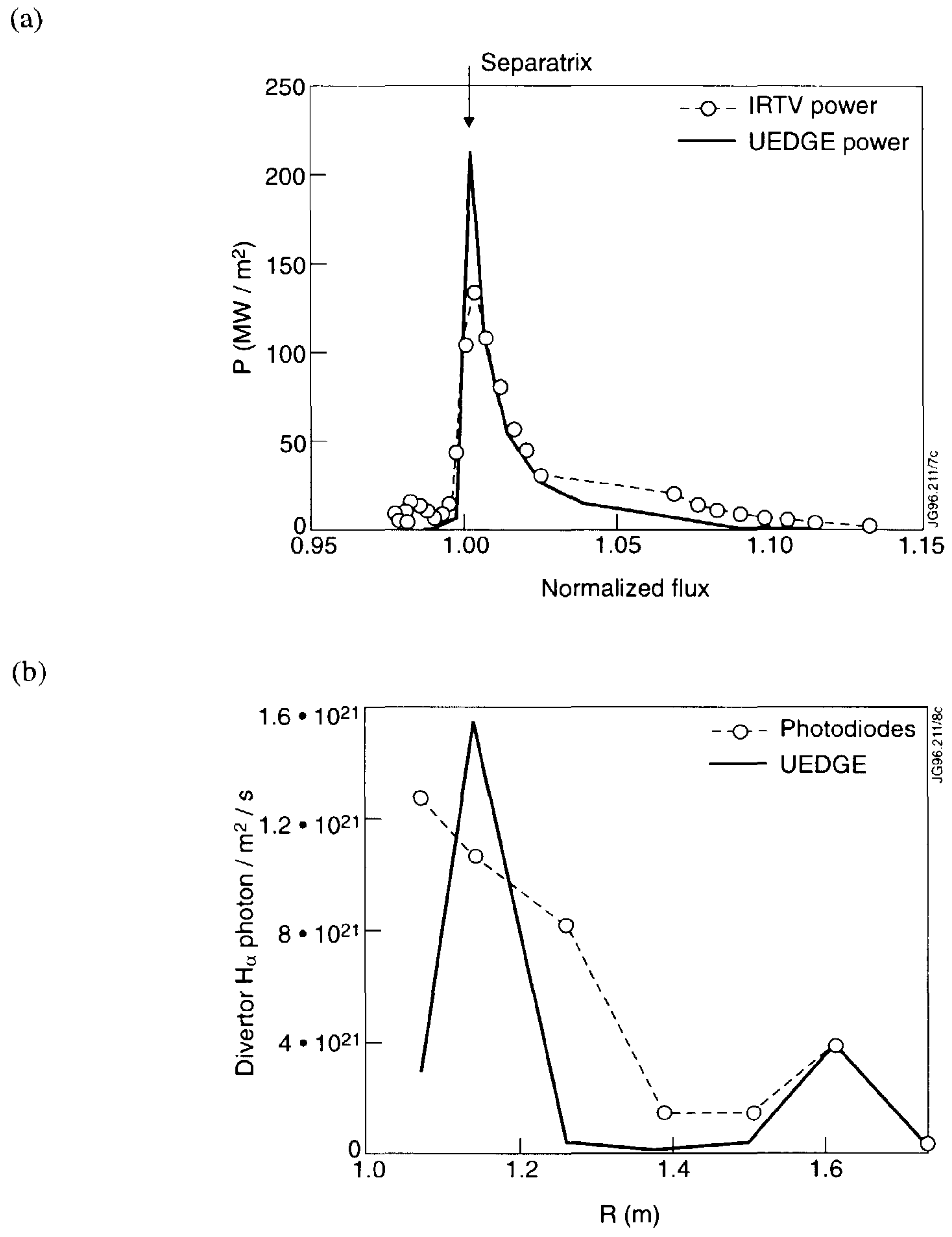

Fig.2. a. Divertor measured and UEDGE modelled parallel power flux for a DIII-D ELMy H-mode discharge versus normalised magnetic flux. b. Divertor measured and UEDGE modelled divertor H_α emission for a DIII-D ELMy H-mode discharge versus major radius at the divertor target.

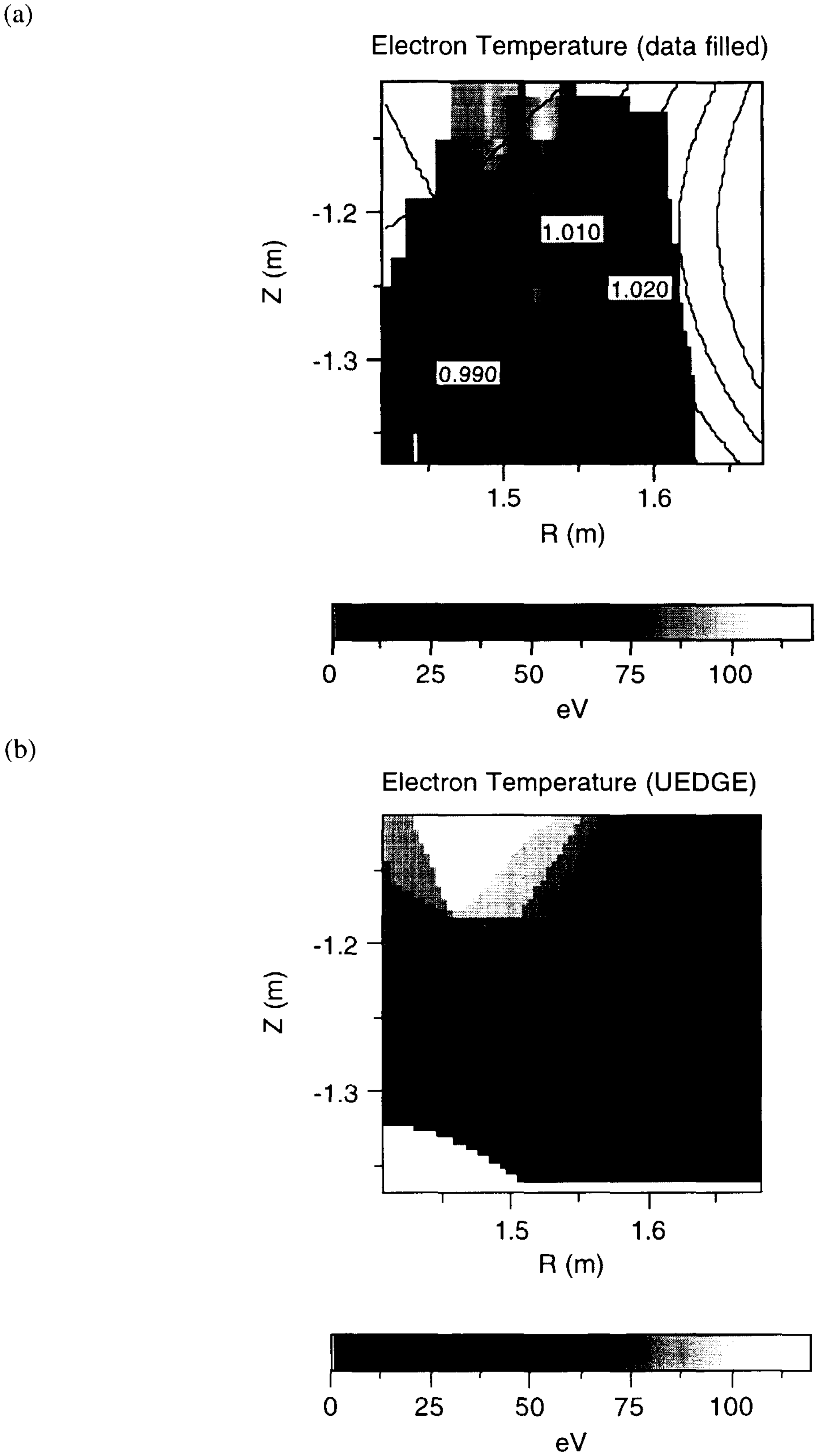

Fig.3. a. Measured electron temperature at the divertor region with Thomson scattering for a DIII-D ELMy H-mode Discharge. b. Electron temperature at the divertor region calculated with UEDGE for this DIII-D ELMy H-mode Discharge.

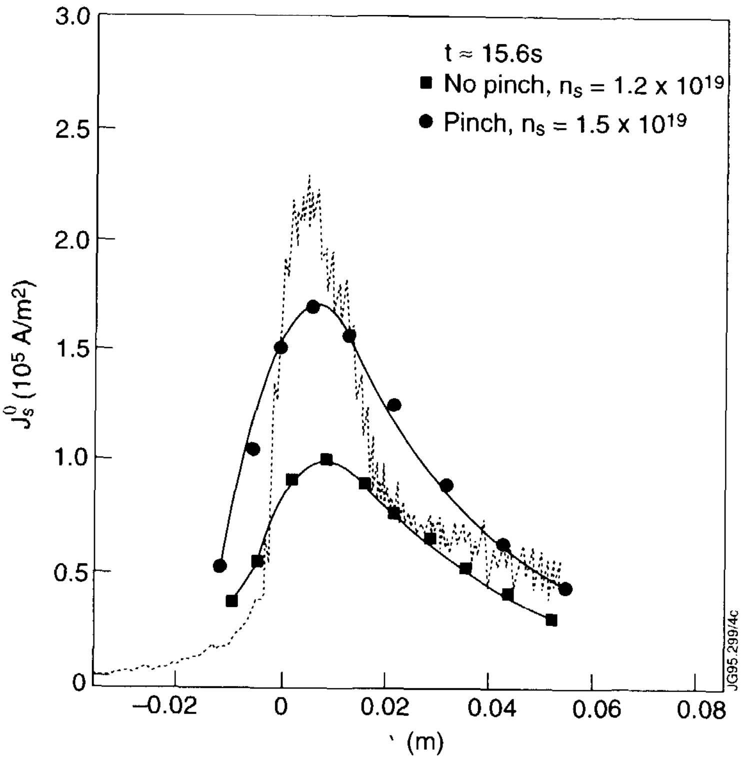

Fig.4. Measured and calculated (EDGE2D/U-NIMBUS, with a constant diffusion coefficient ($D_\perp$= 0.12 m^2/s) and with an inwards SOL particle pinch ($D_\perp$= 1.0 m^2/s, $v_\perp$= 15 m/s)), ion flux profiles for a JET Ohmic high recycling divertor discharge.

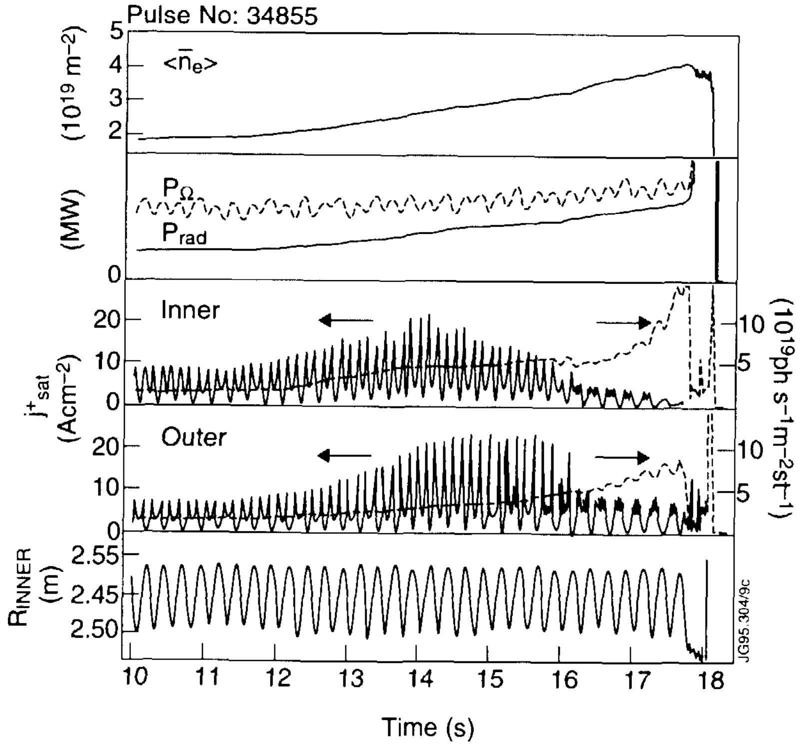

Fig.5. Overview of main plasma and divertor parameters for a JET Ohmic density ramp to detachment. The modulation in the ion flux (j_{sat}) measurements is due to the strike point sweeping performed during the discharge.

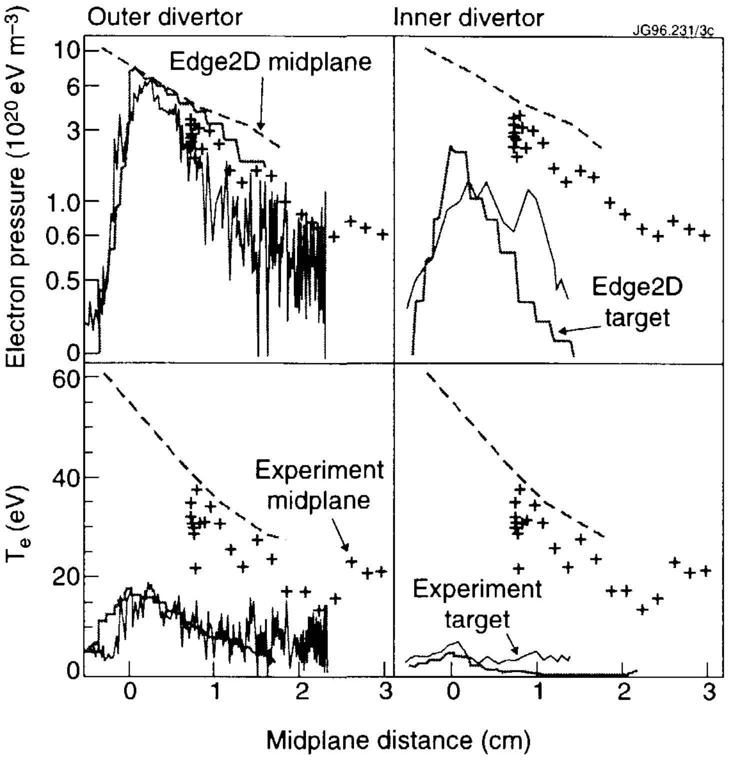

Fig.6. Measured and calculated (EDGE2D/U-NIMBUS) SOL and divertor electron pressure and temperature for a JET L-mode discharge versus distance from the separatrix at the outer midplane. The outer divertor is attached at this stage, while the inner divertor is already detached. The pressure balance method with the outer divertor measurements is used to determine precisely the relative position of the upstream measurements with respect to the magnetic separatrix.

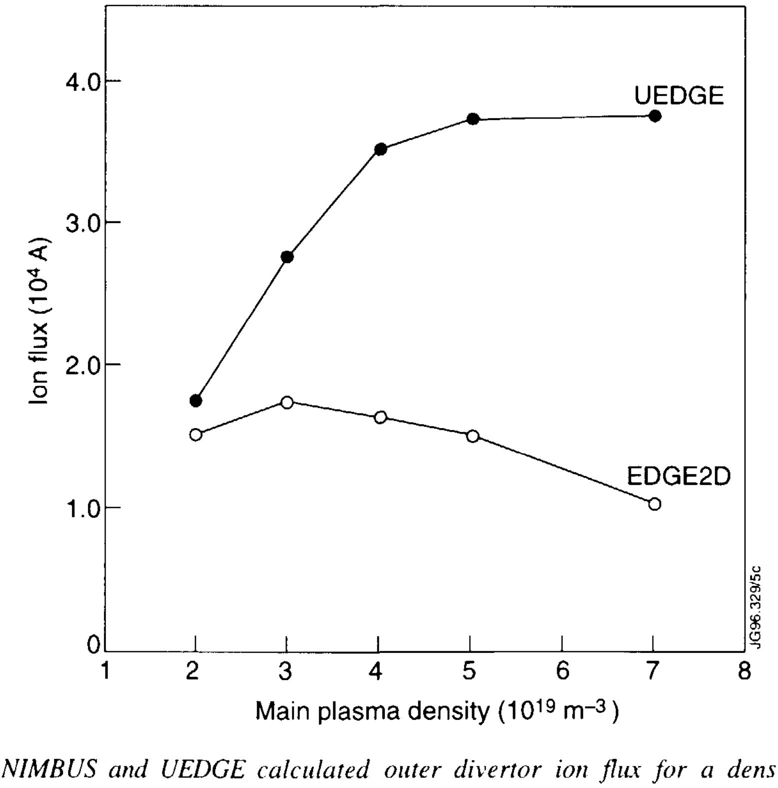

Fig.7. EDGE2D/U-NIMBUS and UEDGE calculated outer divertor ion flux for a density scan in typical JET L-mode conditions.

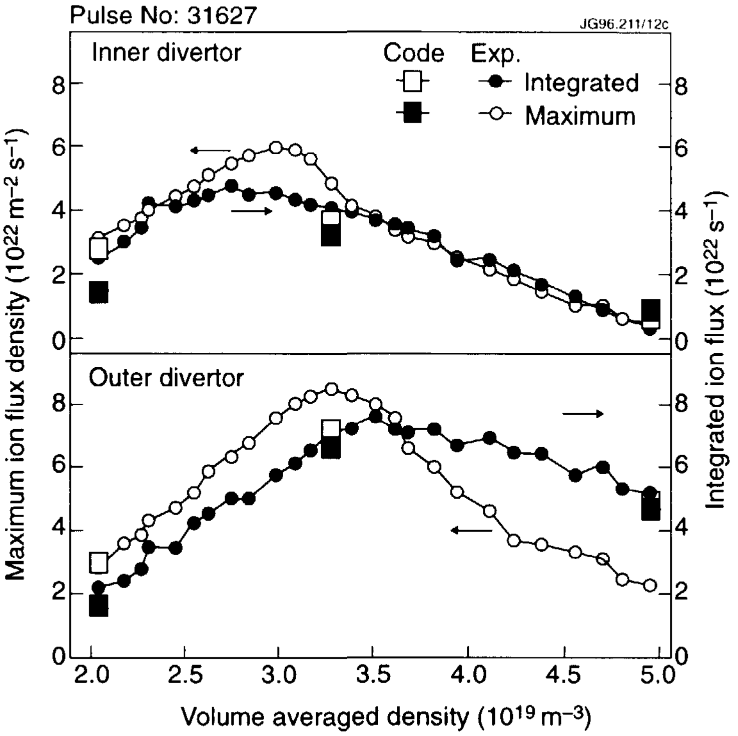

Fig.8. Peak and integral ion fluxes to the inner and outer divertor in JET for an Ohmic density scan and the corresponding results from EDGE2D/U-NIMBUS at the low recycling, high recycling and detached divertor regimes.

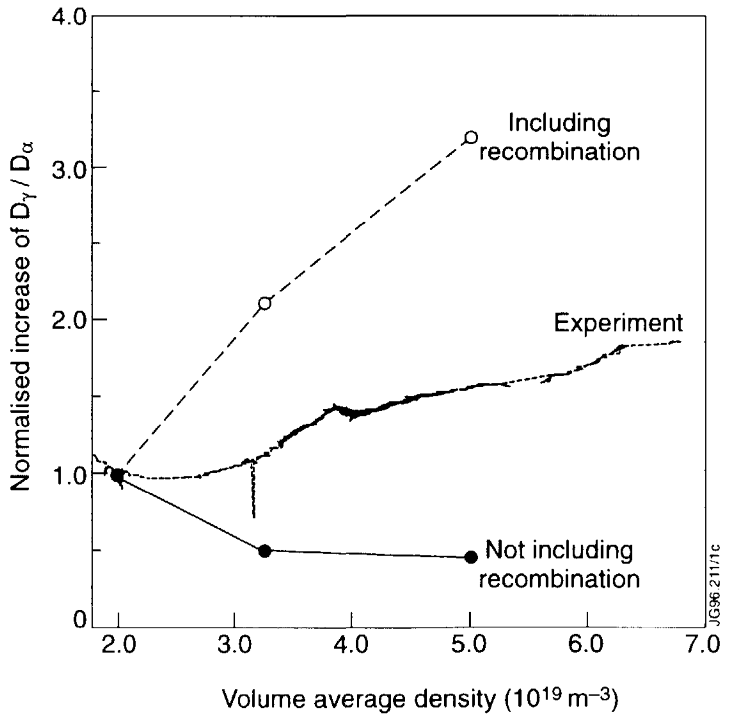

Fig.9. Normalised D_γ/D_α ratio for a density scan to detachment in a JET Ohmic discharge. The computed values from the EDGE2D/U-NIMBUS calculations of Fig. 8 with and without recombination are shown, for comparison.

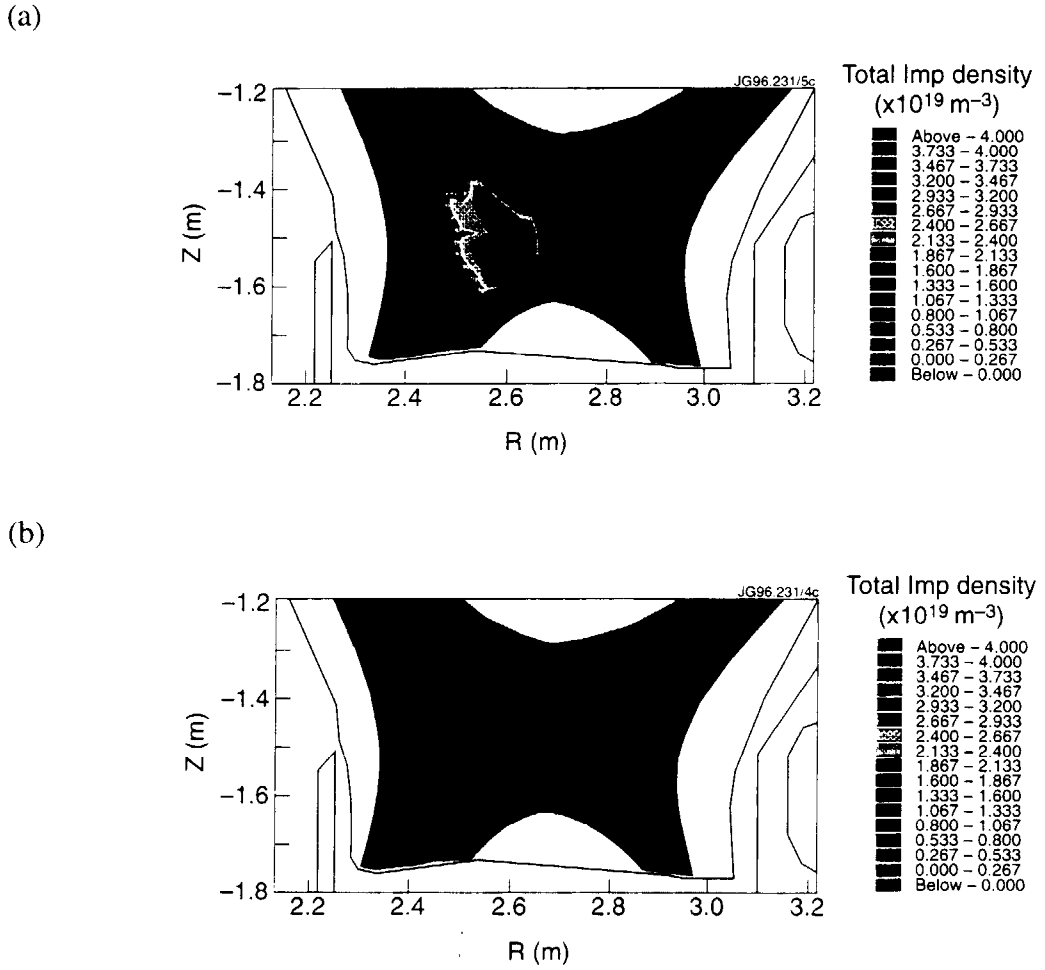

Fig.10. Calculated (EDGE2D/U-NIMBUS) carbon impurity density profiles for a detached (inner) divertor plasma (a) and an attached divertor plasma (b).

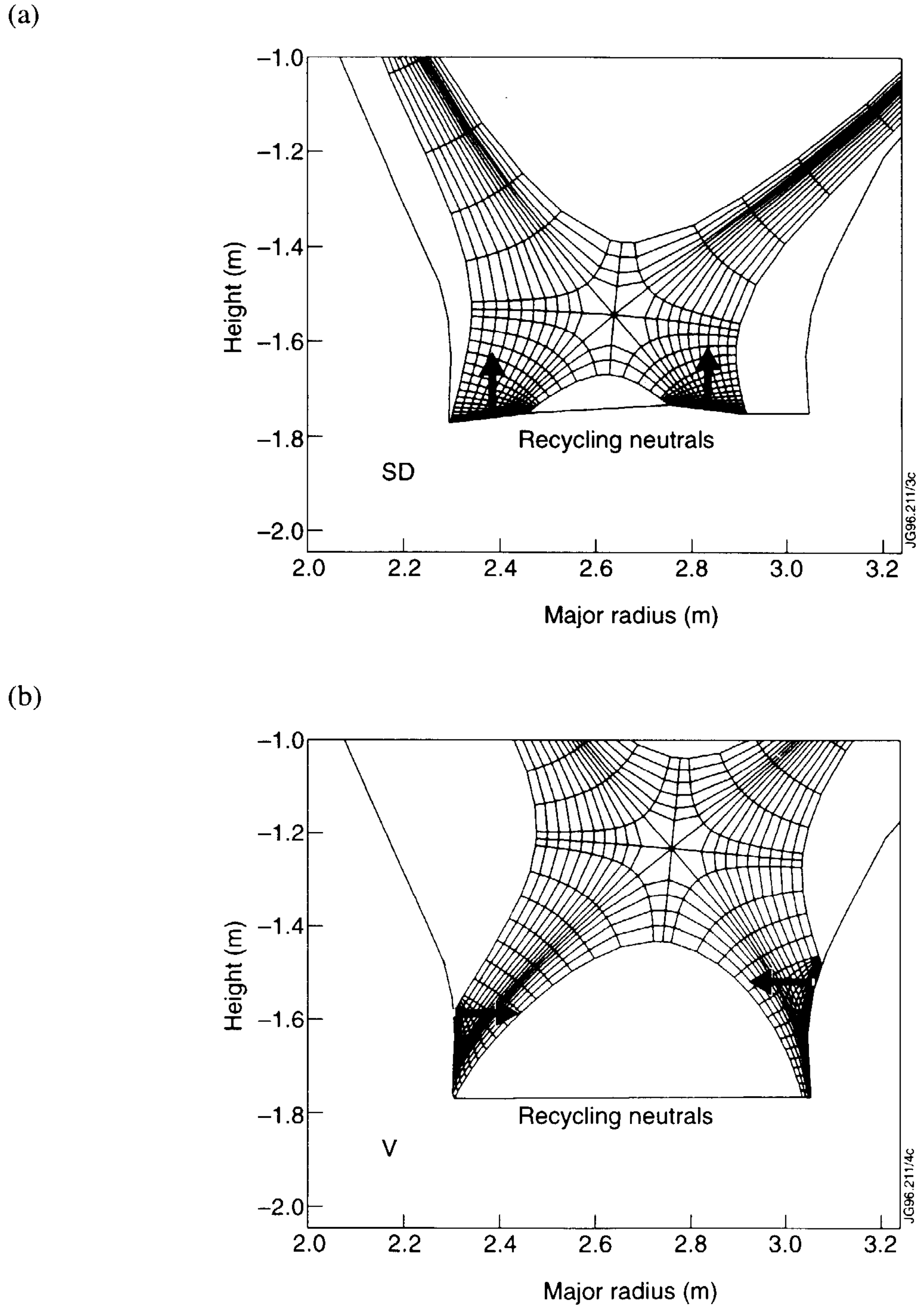

Fig.11. Horizontal (a) and Vertical (b) divertor configurations showing the effect of the divertor geometry on neutral recycling.

(a)

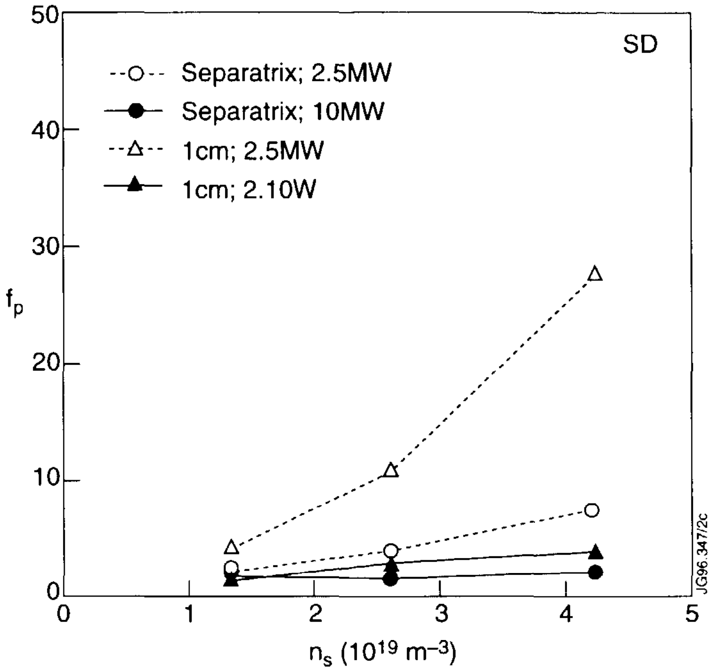

(b)

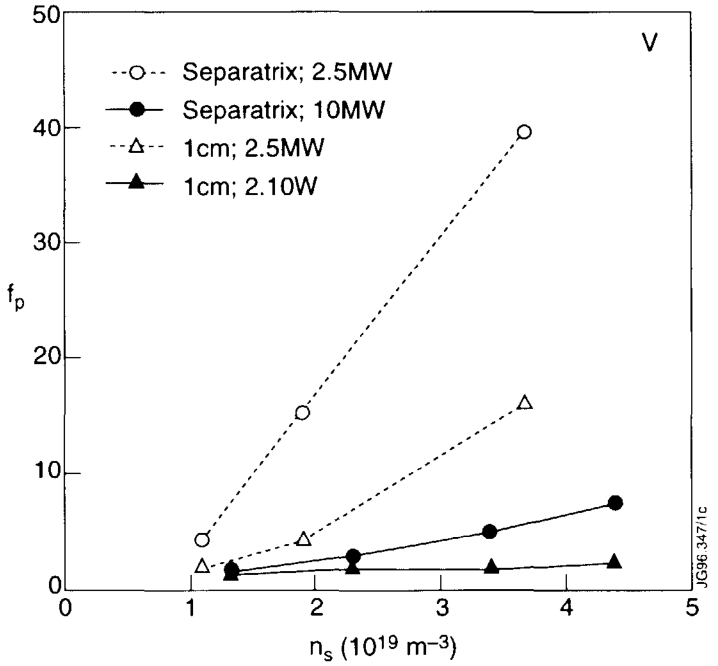

Fig.12. Horizontal (a) and Vertical (b) calculated (EDGE2D/U-NIMBUS) pressure drops for JET conditions versus separatrix density. The pressure drop at the separatrix and the line at a distance of 1 cm at the outer midplane are shown for comparison.

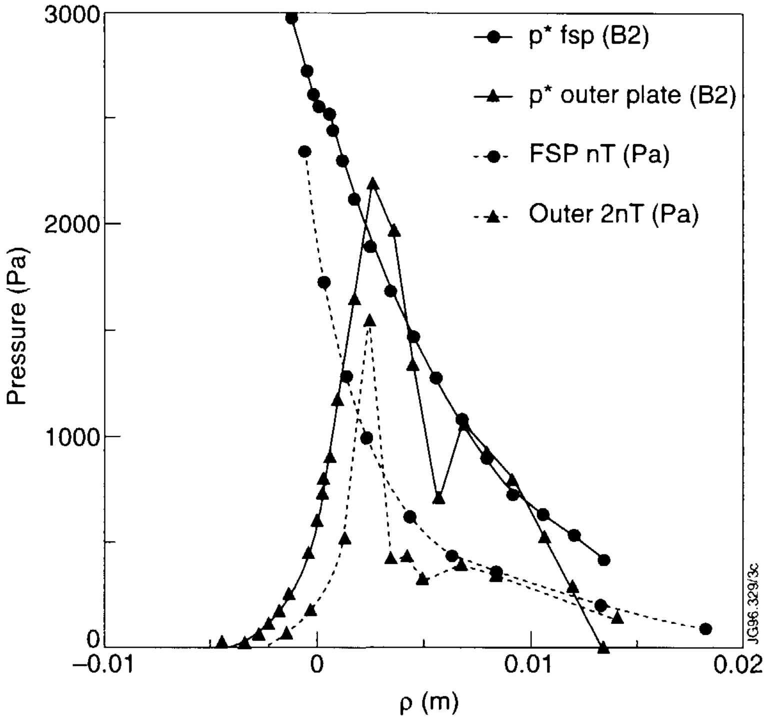

Fig.13. Measured/Calculated (B2-EIRENE) upstream (FSP) and divertor (Outer) pressure, versus distance at the outer midplane, for an Alcator C-mod discharge, showing the plasma over-pressure at the divertor near the separatrix.

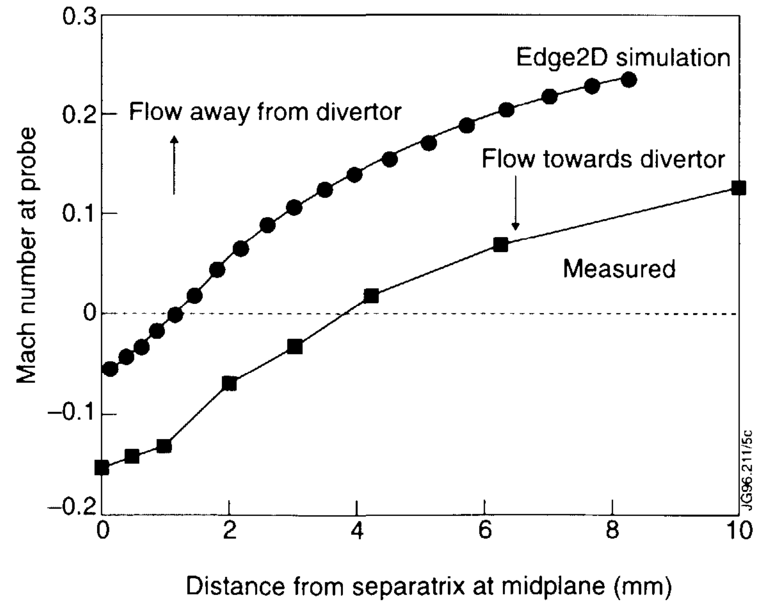

Fig.14. Measured and calculated (EDGE2D/U-NIMBUS) Mach number of the plasma flow at the scanning probe position versus distance at the outer midplane for an Alcator C-mod ohmic discharge. Positive Mach numbers correspond to plasma flow towards the divertor while negative Mach numbers indicate flow reversal.

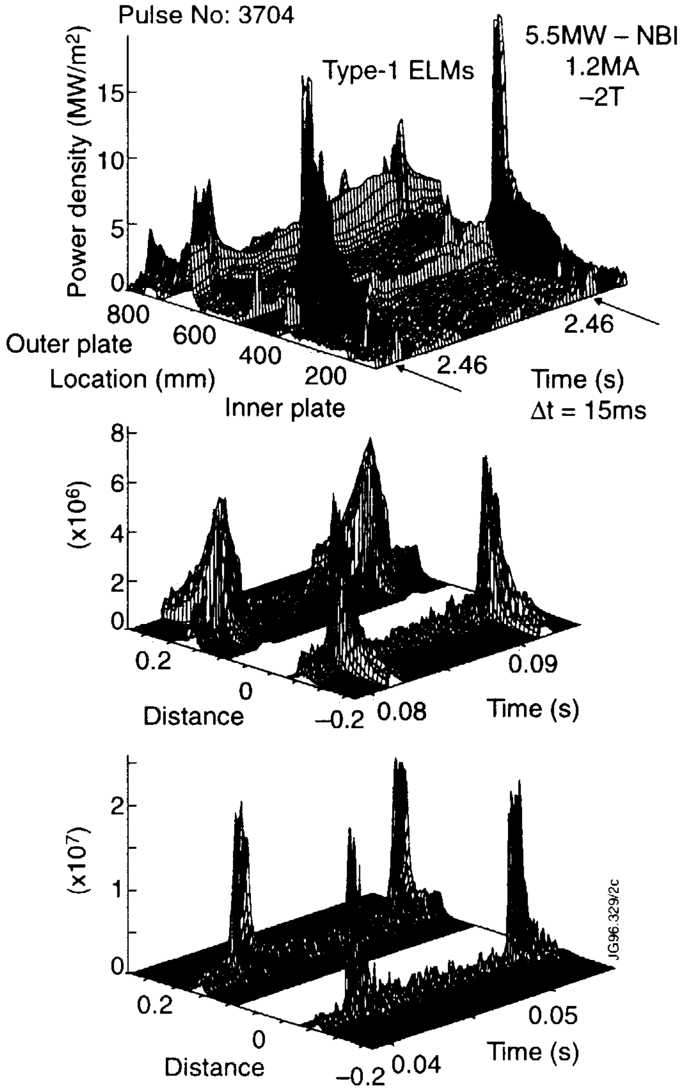

Fig.15. Measured (Top profiles) and calculated (B2-EIRENE) power deposition on the divertor for an ELMy-H-mode discharge in ASDEX-Upgrade. Two simulations are shown : one where the transport coefficients are increased in the main plasma and the SOL (Centre profiles) and the other where the transport coefficients are only increased in the main plasma (Bottom profiles)

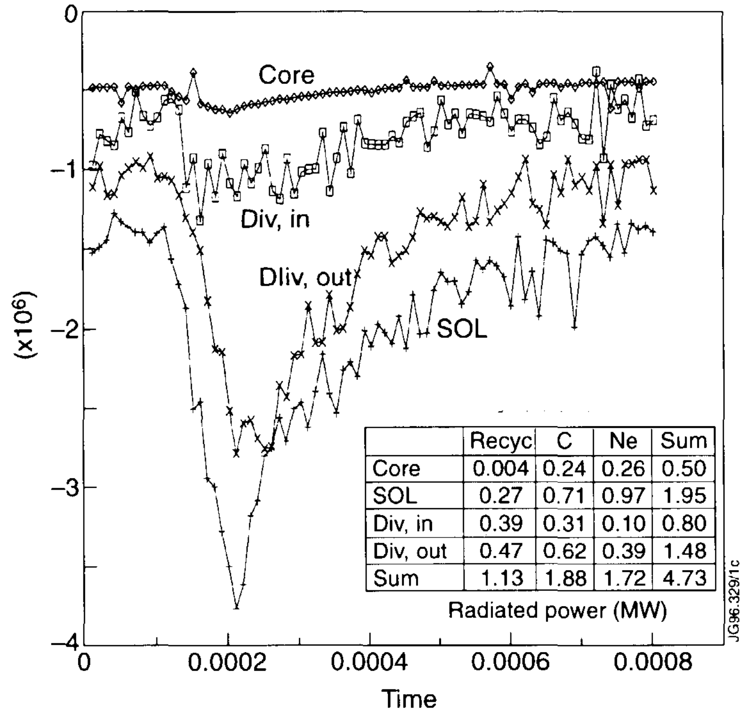

	Recyc	C	Ne	Sum
Core	0.004	0.24	0.26	0.50
SOL	0.27	0.71	0.97	1.95
Div, in	0.39	0.31	0.10	0.80
Div, out	0.47	0.62	0.39	1.48
Sum	1.13	1.88	1.72	4.73

Radiated power (MW)

Fig.16. Modelled radiative losses (B2-EIRENE) in various regions (core, SOL, inner divertor and outer divertor) during a type III ELM for a Radiative H-mode simulation of an ASDEX-Upgrade discharge. Average losses in these regions form hydrogen, carbon and neon are summarised in the inset table.

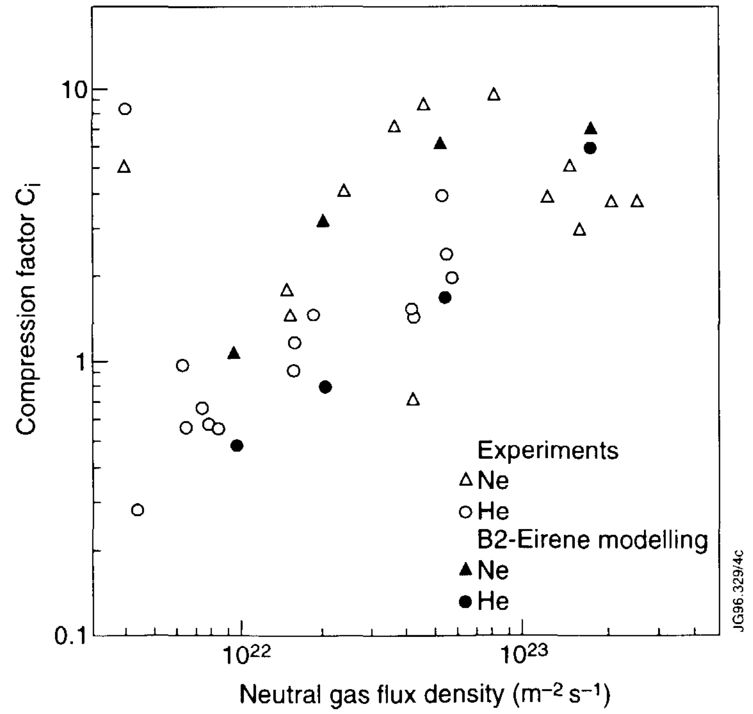

Fig.17. Measured and calculated (B2-EIRENE) neon and helium compression for typical ASDEX-Upgrade ELMy H-mode and Radiative H-mode conditions. The compression factor is defined as

$$C_i = n_i^{\text{neutrals,div}} / n_i^{\text{ions, main plasma edge}} .$$